Voltage recovery influence on three-phase grid-connected inverters under voltage sags

A. Rolán[1,*], P. Giménez[1], S. J. Yagüe[1], S. Bogarra[2], J. Saura[2], M. Bakkar[2]

[1]Department of Industrial Engineering, IQS-URL, Via Augusta 390, Barcelona 08017, Spain
[2]Department of Electrical Engineering, ETSEIAT-UPC, Colom St. 1, Terrassa (Barcelona) 08222, Spain
[*]alejandro.rolan@iqs.url.edu

Abstract: Faults in power systems cause voltage sags, which, in turn, provoke large current peaks in grid-connected equipment. Then, a complete knowledge of the inverter behaviour is needed to meet fault ride-through capability. The aim of this paper is to propose a mathematical model that describes the behaviour of the currents that a three-phase inverter with *RL* filter inject to a faulty grid with symmetrical and unsymmetrical voltage sags. The voltage recovery process is considered, i.e., the fault is assumed to be cleared in the successive zero-cross instants of the fault current. It gives rise to a voltage recovery in different steps (discrete voltage sag), which differs from the usual model in the literature, where the voltage recovers instantaneously (abrupt voltage sag). The analytical model shows that the fault-clearing process has a strong influence on the injected currents. Different sag durations and depths have also been considered, showing that there exist critical values for these magnitudes, which provoke the highest current peaks. The analytical study is validated through simulations in MATLAB[TM] and through experimental results.

1. Introduction

Nowadays, there has been a noticeable increase in the penetration of renewable energy systems into the main grid, whose percentage could reach up to 80% by 2050 [1]. This will imply a new scenario as far as power generation is concerned: the traditional high power stations based on nuclear, thermal or hydro power will reduce their importance, as renewable energy systems will increase its contribution into power generation. This will cause a noticeable reduction in the CO_2 emissions due to the combustion of carbon-based fuels, but it has the drawback that the new power generation units will not be as robust as the traditional ones under grid disturbances. Certainly, high-power synchronous machines used for electricity generation in traditional power stations have strong inertia, so they can get over faults in power systems with relatively no malfunction. However, when a renewable energy system is connected to the grid, it becomes "weak" under electrical disturbances, as there exist no inertia. Moreover, the critical point is the three-phase inverter, as this device couples the DC-link (where the energy delivered from the renewable energy source is stored) with the main grid. In order to get over this shortage in renewable energy systems, control techniques have been proposed in the literature.

Among all grid disturbances, voltage sags are the most common ones [2]. They are mainly caused by faults in power systems, which can cause a reduction in the rms magnitude in one or two phases (unsymmetrical voltage sags) or in the three phases (symmetrical voltage sags). Studies in the literature reveal that large current and torque peaks appear on grid-connected equipment, such as transformers [3] or induction motors [4]-[5]. Protections in power systems are a good solution to tackle the problem [6], but they disconnect the equipment from the grid, thus power

is not sent to the end-users. For this reason, it is important to propose analytical models that help in the understanding of grid-connected equipment under voltage sags with the aim of providing solutions to mitigate the problem without disconnecting the system from the grid (fault ride-through capability).
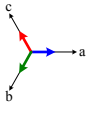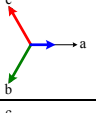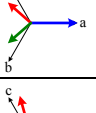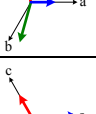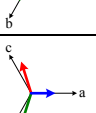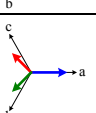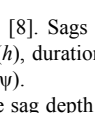
The aim of this paper is not to provide a robust or a sound control for grid-connected renewable energy systems (a summary of these control techniques, as well as the grid interconnection issues between wind and photovoltaic systems and the grid can be found in [7]). This paper focuses on the study that the voltage recovery process cause on grid-connected inverters, because it gives rise to less severe effects than when sags are assumed to be cleared instantaneously. Then, the instantaneous voltage recovery process (*abrupt* sag) overestimates the sag severity, while if the voltage recovery process takes into account the successive zero-cross instants of the fault current (*discrete* sag), the sag severity is weakened, which is what it happens in real applications.

This paper is structured as follows. Firstly, a description of voltage sags and the voltage recovery process is given. Secondly, the analytical model of a three-phase grid-connected inverter with an *RL* filter is carried out when subject to either symmetrical or unsymmetrical voltage sags. Thirdly, the sag parameters influence (duration and depth) is analyzed. Finally, the analytical study has been validated through simulations in MATLAB[TM] and experimental results.

2. Voltage sags

Voltage sags are the grid disturbances originated mainly by faults, which cause a decrease in the rms voltage with respect to the steady-state pre-fault voltage from 0.1 pu and 0.9 pu and the usual durations go from 0.5 cycles and 1

1

Table 1 Voltage sags: types, phasors and sequence components (adapted from [2]) and voltage recovery process (adapted from [9])

Type	Phasors	Zero seq.	Positive seq.	Negative seq.	Voltage Recovery Process			
					Type	First recovery (ωt_{f1})	Second recovery (ωt_{f2})	Third recovery (ωt_{f3})
A		$\underline{V}_A^0 = 0$	$\underline{V}_A^+ = h\underline{V}$	$\underline{V}_A^- = 0$	A_1	$n\,180° - \alpha_a + \psi - 90°$	$n\,180° - \alpha_a + \psi$	—
					A_2	$n\,180° - \alpha_a + \psi$	$n\,180° - \alpha_a + \psi + 90°$	—
					A_3	$n\,180° - \alpha_a + \psi - 90°$	$n\,180° - \alpha_a + \psi - 30°$	$n\,180° - \alpha_a + \psi + 30°$
					A_4	$n\,180° - \alpha_a + \psi$	$n\,180° - \alpha_a + \psi + 60°$	$n\,180° - \alpha_a + \psi + 120°$
					A_5	$n\,180° - \alpha_a + \psi - 90°$	$n\,180° - \alpha_a + \psi - 90°$	$n\,180° - \alpha_a + \psi + 30°$
B		$\underline{V}_B^0 = -\dfrac{1-h}{3}\underline{V}$	$\underline{V}_B^+ = \dfrac{2+h}{3}\underline{V}$	$\underline{V}_B^- = -\dfrac{1-h}{3}\underline{V}$	B	$n\,180° - \alpha_a + \psi - 90°$	—	—
C		$\underline{V}_C^0 = 0$	$\underline{V}_C^+ = \dfrac{1+h}{2}\underline{V}$	$\underline{V}_C^- = \dfrac{1-h}{2}\underline{V}$	C	$n\,180° - \alpha_a + \psi$	—	—
D		$\underline{V}_D^0 = 0$	$\underline{V}_D^+ = \dfrac{1+h}{2}\underline{V}$	$\underline{V}_D^- = -\dfrac{1-h}{2}\underline{V}$	D	$n\,180° - \alpha_a + \psi - 90°$	—	—
E		$\underline{V}_E^0 = \dfrac{1-h}{3}\underline{V}$	$\underline{V}_E^+ = \dfrac{1+2h}{3}\underline{V}$	$\underline{V}_E^- = \dfrac{1-h}{3}\underline{V}$	E_1	$n\,180° - \alpha_a + \psi + 30°$	$n\,180° - \alpha_a + \psi + 150°$	—
					E_2	$n\,180° - \alpha_a + \psi + 150°$	$n\,180° - \alpha_a + \psi - 150°$	—
F		$\underline{V}_F^0 = 0$	$\underline{V}_F^+ = \dfrac{1+2h}{3}\underline{V}$	$\underline{V}_F^- = -\dfrac{1-h}{3}\underline{V}$	F_1	$n\,180° - \alpha_a + \psi + 120°$	$n\,180° - \alpha_a + \psi - 120°$	—
					F_2	$n\,180° - \alpha_a + \psi + 60°$	$n\,180° - \alpha_a + \psi + 120°$	—
G		$\underline{V}_G^0 = 0$	$\underline{V}_G^+ = \dfrac{1+2h}{3}\underline{V}$	$\underline{V}_G^- = \dfrac{1-h}{3}\underline{V}$	G_1	$n\,180° - \alpha_a + \psi + 30°$	$n\,180° - \alpha_a + \psi + 150°$	—
					G_2	$n\,180° - \alpha_a + \psi + 150°$	$n\,180° - \alpha_a + \psi - 150°$	—

minute [8]. Sags are characterized by four parameters [2]: depth (*h*), duration (Δ*t*), phase-angle jump and fault current angle (ψ).

The sag depth (*h*) is defined for symmetrical sags as the remaining voltage with respect to the pre-fault steady-state voltage, and for unsymmetrical sags it is defined for radial feeders after applying a voltage divider for the positive- and negative-components [2]. The fault current angle indicates the origin of voltage recovery, as it is defined as the instant when fault current crosses zero. It varies between 75º and 85º for transmission systems [9]. In this paper, the three-phase inverter is assumed to be connected at the transmission level, so a fault current angle of ψ = 80º is considered. Moreover, for transmission grids it is possible to neglect the phase-angle jump [2]. Finally, the duration is defined as the time that goes from the instant in which the sag is originated until the instant in which the last phase of the protections clear the fault. It should be noted that in the literature this fault-clearing process is assumed to be done instantaneously, while what it really happens is that the protection system acts at the instants where the fault current crosses zero. It gives rise to a voltage recovery process which can be done in one, two, or three steps, as indicated in

Table 1.

Table 1 shows the sag classification with the expressions for the zero-, positive-, and negative-sequence components (adapted from [2]) and the voltage recovery process (adapted from [9]). Type A sags are the symmetrical sags, which are originated by 3-phases or 3-phases-to-ground faults, causing the same voltage reduction in the three phases. Unsymmetrical sags are a voltage reduction which is different for the three phases and they are classified into seven types, according to the cause of origin: B (1-phase-to-ground fault); C (2-phases fault or 1-phase-to-ground fault after a Dy transformer); D (2-phases fault after a Dy transformer o 1-phase-to-ground fault after two Dy-transformers); E (2-phases-to-ground fault); F (2-phases-to-ground fault after a Dy transformer); and G (2-phases-to-ground fault after two Dy-transformers). All these sags have an instantaneous voltage recovery, and they are named *abrupt* sags.

With respect to the voltage recovery process, Table 1 shows that there are 14 types of *discrete* voltage sags: 5 symmetrical sags (A_1, A_2, A_3, A_4, and A_5) plus 9 unsymmetrical sags (B, C, D, E_1, E_2, F_1, F_2, G_1 and G_2). However, the authors' previous work [10] demonstrated that
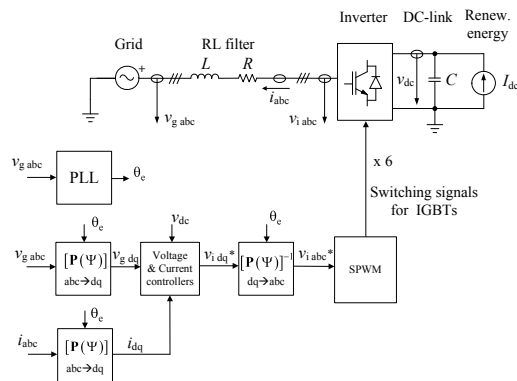
2

Fig. 1 *General scheme of a three-phase inverter with* RL *filter connected to the main grid and its control. Generator-sign convention*

when studying the behaviour of grid-connected equipment under voltage sags the following group of voltage sags cause the same behaviour in the electrical variables: A_1-A_2, A_4-A_5, C-D, F_1-G_1 and F_2-G_2. As a result, for the present paper only the following sags are considered: symmetrical sag types A_1 and A_4, and unsymmetrical sag types C, F_1 and F_2.

3. Three-phase grid-connected inverters

Fig. 1 shows the general scheme of a three-phase inverter connected to a grid. The DC-link consists of a capacitor (C), which is fed by a DC current source (I_{dc}), which models the renewable energy conversion system. This DC voltage is transformed into AC voltage by means of a proper control of the inverter, whose output voltage ($v_{i\,abc}$) is not sinusoidal, thus a filter is needed to reduce the total harmonic distortion (THD). The selected filter for the present paper is a *RL* filter, which simplifies the analytical study, although there are other possibilities, such as the *LCL* filter [11].

It is observed from Fig. 1 that the control system works in *dq* variables, which are the *direct* and *quadrature* components after applying *Park*'s transformation [12] to the *abc* variables. The *dq* variables are usually obtained in the synchronous reference frame. To this end, a phase-locked loop (PLL) [13] obtains the angle of the grid voltages in order to make the system be in synchronism with them. The proper control of the v_{dc} voltage and the i_{dq} currents give the reference values for the *abc* inverter voltages. These voltages are compared with a carrier triangular wave by means of the sinusoidal pulse-width modulation (SPWM) technique [14]. The result of the SPWM gives the switching pattern for the 6 IGBTs of the inverter.

An interesting compilation among the different controls in the literature and the problems related to the grid synchronization of renewable energies can be found in [1]. Control algorithms to be used for three-phase inverter under unbalanced grid conditions, i.e., under unsymmetrical sags can be found, among others, in [15], which are based in a proper calculation of the reference values for the positive- and negative-sequence components of *dq* currents according to the instantaneous power theory developed in [16]. Note that the aim of this work is not to propose an improved

control to the three-phase inverter, but to develop an analytical study.

4. Analytical study

4.1. Injected current solution in complex form

The mathematical study is developed using the complex form of the *dq* variables, as they provide a compact form for the electrical expressions, which eases the task to obtain an analytical solution to the problem. This is done by applying the *Ku* transformation (see Appendix II for more details).

The mathematical expressions that model the system of Fig. 1 (considering the generator-sign convention) are:

$$\begin{bmatrix} v_{ia} \\ v_{ib} \\ v_{ic} \end{bmatrix} = \begin{bmatrix} R & 0 & 0 \\ 0 & R & 0 \\ 0 & 0 & R \end{bmatrix} \begin{bmatrix} i_a \\ i_b \\ i_c \end{bmatrix} + \frac{d}{dt} \begin{bmatrix} L & 0 & 0 \\ 0 & L & 0 \\ 0 & 0 & L \end{bmatrix} \begin{bmatrix} i_a \\ i_b \\ i_c \end{bmatrix} + \begin{bmatrix} v_{ga} \\ v_{gb} \\ v_{gc} \end{bmatrix}. \quad (1)$$

If we apply the *Ku* transformation in the synchronous reference frame (equation (19) in Appendix II) to the matrix system (1), we obtain the following expression:

$$v_{if} = \left[R + L(s + j\omega) \right] i_f + v_{gf} \quad (2)$$

where v_{if} is the transformed voltage at the inverter output, R and L are the filter resistance and the filter inductance, respectively, s = d/dt is the derivative operator, $\omega = 2\pi f$ is the pulsation of the grid voltages ($f = 1/T$ is the grid frequency and T is its period), i_f is the transformed current that the inverter injects to the grid, and v_{gf} is the transformed grid voltage, which is given by the following equation (according to (22) in Appendix II) under unbalanced conditions:

$$v_{gf} = v_{gf}^+ + v_{gf}^- e^{-j2\omega t} \quad (3)$$

and according to (25) in Appendix II, v_{gf}^+ and v_{gf}^- are:

$$v_{gf}^+ = \sqrt{3/2}\,\underline{V}^+ \qquad ; \qquad v_{gf}^- = \sqrt{3/2}\left(\underline{V}^-\right)^* \quad (4)$$

being $\underline{V}^+$ and $\underline{V}^-$ the positive- and negative-sequence components of sags shown in Table 1. Then, the differential equation of the transformed current can be obtained from (2) considering the transformed grid voltage (3), resulting in:

$$s i_f = \frac{1}{L} \left[v_{if} - \left(v_{gf}^+ + v_{gf}^- e^{-j2\omega t} \right) - (R + j\omega L) i_f \right]. \quad (5)$$

In order to find an analytical solution for (5), the following assumption is made: the control systems is able to set the transformed inverter voltage (v_{if}) constant in the synchronous reference frame at its pre-fault steady-state value. By doing this, (5) is a first-order ODE with constant coefficients. Its solution will be the *homogenous* solution plus the *particular* solution. The *homogeneous* solution is obtained by neglecting the excitations of (5), i.e. $v_{if} = v_{gf}^+ = v_{gf}^- e^{-j2\omega t} = 0$, giving:

$$i_{f\,homog} = \underline{K}\,e^{-(R/L)t}\,e^{-j\omega t}. \quad (6)$$

And the *particular* solution is the steady-state solution

3

Inverter + *RL* filter

Faulty grid

S_1 i_{f1} Eq. (12)
t_{ON}: $t < t_i$

S_2 i_{f2} Eq. (13)
t_{ON}: $t_i \leq t < t_f$

S_3 i_{f3} Eq. (15)
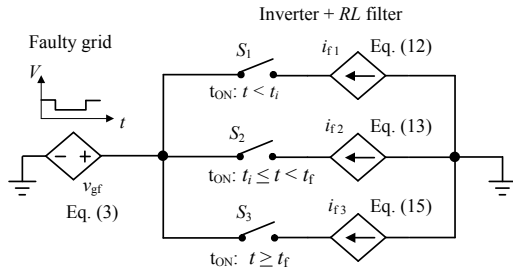t_{ON}: $t \geq t_f$

V

v_{gf}
Eq. (3)

Fig. 2 *Proposed electrical model for a three-phase inverter with* RL *filter under a faulty grid*

of (5), which can be expressed as:

$$i_{f\,part} = i_{f\,part}^{+} + i_{f\,part}^{-}\,e^{-j2\omega t} \qquad (7)$$

where $i_{f\,part}^{+}$ is the steady-state solution (s = 0) of (5) with no negative-sequence voltage ($v_{gf}^{-} = 0$), and $i_{f\,part}^{-}$ is the steady-state solution of (5) with no positive-sequence voltage ($v_{if} = v_{gf}^{+} = 0$), which results in:

$$i_{f\,part}^{+} = \frac{v_{if} - v_{gf}^{+}}{R + j\omega L} \quad ; \quad i_{f\,part}^{-} = -\frac{v_{gf}^{-}}{R - j\omega L} \qquad . \qquad (8)$$

Finally, the solution of the first-order ODE (5) is the addition of the *homogenous* solution (6) plus the *particular* solution (7)-(8), resulting in:

$$i_f = \underline{K}\,e^{-(R/L)t}\,e^{-j\omega t} + \frac{v_{if} - v_{gf}^{+}}{R + j\omega L} - \frac{v_{gf}^{-}}{R - j\omega L}e^{-j2\omega t} \qquad . \qquad (9)$$

The complex constant $\underline{K}$ is obtained by means of the initial conditions (at $t = t_0$, the initial transformed current is $i_f = i_{f0}$):

$$\underline{K} = \left(i_{f0} + \frac{v_{gf}^{+} - v_{if}}{R + j\omega L} + \frac{v_{gf}^{-}}{R - j\omega L}e^{-j2\omega t_0} \right)e^{(R/L)t_0}\,e^{j\omega t_0} \qquad . \qquad (10)$$

Finally, substituting (10) in (9) gives:

$$i_f = \left(i_{f0} + \frac{v_{gf}^{+} - v_{if}}{R + j\omega L} + \frac{v_{gf}^{-}}{R - j\omega L}e^{-j2\omega t_0} \right)e^{-\left(\frac{R}{L}\right)(t-t_0)}\,e^{-j\omega(t-t_0)}$$
$$+ \frac{v_{if} - v_{gf}^{+}}{R + j\omega L} - \frac{v_{gf}^{-}}{R - j\omega L}e^{-j2\omega t} \qquad . \qquad (11)$$

4.2. State 1: Before the sag (t < t_i)

It is assumed that the system operates at its steady-state before the sag is originated at $t = t_i$. So, the positive-sequence component for the transformed grid voltage equals its steady state value ($v_{gf}^{+} = v_{gf\,st}$) and there is no negative-sequence voltage ($v_{gf}^{-} = 0$). So, the steady-state expression for (11) is:

$$i_{f1} = \frac{v_{if} - v_{gf\,st}}{R + j\omega L} \quad ; \quad (t < t_i) \qquad . \qquad (12)$$

4.3. State 2: During the sag (t_i ≤ t < t_f)

The voltage sag starts at $t = t_i$ and ends at $t = t_f$. The initial transformed current for this time interval is (12), which substituted in (11) results in:

$$i_{f2} = \underline{K}_1\,e^{-(R/L)(t-t_i)}\,e^{-j\omega(t-t_i)} - \underline{K}_2 e^{-j2\omega t} + \underline{K}_3 \; ; \left(t_i \leq t < t_f \right) (13)$$

where the complex constants $\underline{K}_1$, $\underline{K}_2$ and $\underline{K}_3$ are given by:

$$\underline{K}_1 = \frac{v_{gf}^{+} - v_{gf\,st}}{R + j\omega L} + \underline{K}_2\,e^{-j2\omega t_i} ; \; \underline{K}_2 = \frac{v_{gf}^{-}}{R - j\omega L} ; \; \underline{K}_3 = \frac{v_{if} - v_{gf}^{+}}{R + j\omega L} \qquad . \qquad (14)$$

4.4. State 3: After the sag (t ≥ t_f)

The fault is cleared at $t = t_f$. The initial condition is then given by the current (13) evaluated at $t = t_f$. Moreover, when the sag ends the system goes back to its steady-state operation ($v_{gf}^{+} = v_{gf\,st}$), so there is no negative-sequence voltage ($v_{gf}^{-} = 0$). Substituting these conditions in (11), it results in:

$$i_{f3} = \underline{K}_4\,e^{-(R/L)(t-t_f)}\,e^{-j\omega(t-t_f)} + \underline{K}_5 \quad ; \quad \left(t \geq t_f \right) \qquad (15)$$

where the complex constants $\underline{K}_4$ and $\underline{K}_5$ are given by:

$$\underline{K}_4 = \underline{K}_1\,e^{-(R/L)(t_f-t_i)}\,e^{-j\omega(t_f-t_i)} - \underline{K}_2 e^{-j2\omega t_f} + \underline{K}_6$$
$$\underline{K}_5 = \frac{v_{if} - v_{gf\,st}}{R + j\omega L} \quad ; \quad \underline{K}_6 = \frac{v_{gf\,st} - v_{gf}^{+}}{R + j\omega L} \qquad . \qquad (16)$$

The proposed analytical model consists of equations (12), (13), and (15), which describe the behaviour of a three-phase grid-connected inverter with *RL* filter under unsymmetrical voltage sags. These equations can be represented by the three voltage-controlled current sources depicted in Fig. 2. Note that the presented model is also valid for symmetrical sags (in this case, there is no negative-sequence component, so $v_{gf}^{-} = 0$).

5. Voltage recovery influence

Fig. 3 shows the voltage recovery influence (*abrupt* and *discrete* sags) on the injected currents from the inverter to the grid when faults cause symmetrical sags (type A) and unsymmetrical sag type F. All the simulated sags have a duration $\Delta t = 5.5$ cycles (i.e., 110 ms with $f = 50$ Hz) and a depth $h = 0.8$. Both transformed and real currents are represented in per unit (or pu) values, according to:

$$i_{f\,pu}(t) = i_f(t) / \left(\sqrt{3/2}I_b \right) \quad ; \quad i_{abc\,pu}(t) = i_{abc}(t) / \left(\sqrt{2}I_b \right) (17)$$

where I_b is the current base value ($I_b = I_N$, see Appendix I).

Regarding symmetrical voltage sags, when the sag starts at $t = t_i$, note that the transformed current rotates at pulsation ω: the locus of the transformed current (Fig. 3a) has a circumferential shape and the time evolution of the transformed current (Fig. 3b) shows a pulsation ω during the period of time when the fault occurs. This is due to the exponential term $e^{-j\omega(t-ti)}$ that appears in (13). Note also that when the sag ends at $t = t_f$ if the sag is modelled *abrupt*, then the voltage recovery process is more severe than if it is modelled *discrete*. Indeed, note from Fig. 3c that for type A_1 (*abrupt*), the peak value of the real currents is 1.77 pu, while for type A_1 (*discrete* with two-step voltage recovery) this peak value is 1.48 pu and for type A_4 (*discrete* with three-step voltage recovery) the value is 1.47 pu. It means that as the number of steps in fault-clearing increases, the sag causes less severe effects on the injected currents.
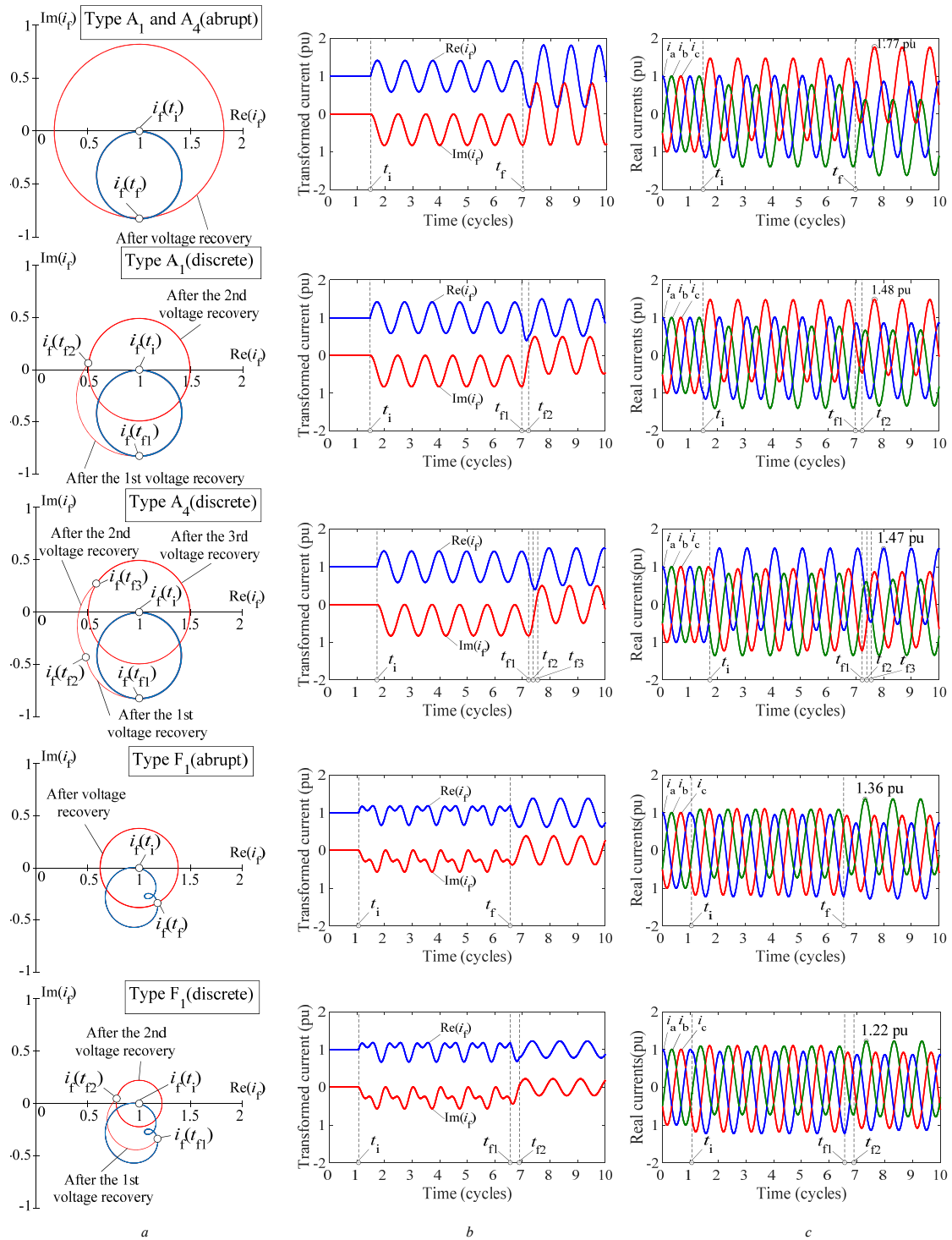
4

Fig. 3 *Voltage recovery influence on the currents injected from the inverter to the grid under symmetrical sag types A_1 and A_4 (abrupt and discrete) and under unsymmetrical sag type F_1 (abrupt and discrete). Sags characteristics: $\Delta t = 5.5$ cycles, $h = 0.8$ and $\psi = 80°$*

a Locus of the transformed current

b Real and imaginary part of the transformed current
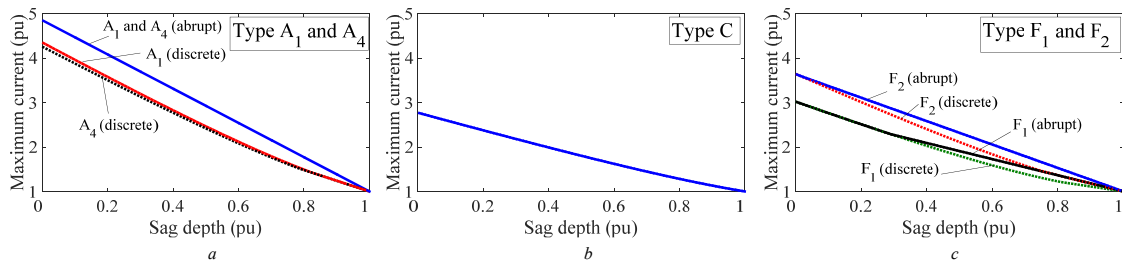
c Three-phase components (abc) of the current

Fig. 4 *Sag depth influence on the maximum current peak. Sags characteristics: Δt = 5.5 cycles, h = 0...1 and ψ = 80°*

a Inverter under symmetrical sag types A_1 and A_4 (abrupt and discrete)

b Inverter under unsymmetrical sag type C

c Inverter under unsymmetrical sag types F_1 and F_2 (abrupt and discrete)

Fig. 5 *Sag duration influence on the maximum current peak. Sags characteristics: Δt = 5...7 cycles, h = 0.8 and ψ = 80°*

a Inverter under symmetrical sag types A1 and A4 (abrupt and discrete)

b Inverter under unsymmetrical sag type C

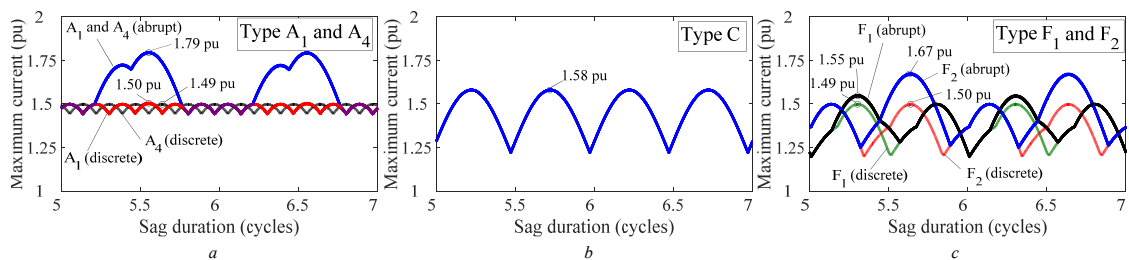*c* Inverter under unsymmetrical sag types F1 and F2 (abrupt and discrete)

This is a logical consequence if we look at the locus of the transformed current shown in Fig. 3a. Note from this figure that if the sag has an *abrupt* voltage recovery process, the value of the transformed current when the sag ends, $i_f(t_f)$, is located in a further position from its pre-fault steady-state value, $i_f(t_i)$. However, when the sag has a *discrete* voltage recovery, the transformed current in the second recovery, $i_f(t_{f2})$, or in the third recovery, $i_f(t_{f3})$, is closer to the pre-fault steady-state value, $i_f(t_i)$.

Regarding unsymmetrical sags (type F_1), note that when the sag starts at $t = t_i$, neither the locus of the transformed current (Fig. 3a) has a circumferential shape, nor the time evolution of the transformed current (Fig. 3b) has a pulsation ω. This is explained by the exponential term that depends on twice the fundamental pulsation, $e^{-j2\omega t}$, which appears in (13). The addition of this term and the term that depends on the fundamental pulsation, $e^{-j\omega(t-t_i)}$, creates a distorted circumferential shape on the locus during the voltage sag (Fig. 3a). However, note that when the voltage sag ends at $t = t_f$, the transformed current has again a circumferential shape in its locus (Fig. 3a) and the fundamental pulsation ω in the time response (Fig. 3b). This is because after voltage recovery, (15) shows that there is no exponential term that depends on twice the fundamental pulsation. Note also from Fig. 3a that, as it happened under symmetrical sags, when unsymmetrical sags are modelled *discrete*, the transformed current after the second voltage recovery, $i_f(t_{f2})$, is closer to its pre-fault steady-state value, $i_f(t_i)$, than in the case of *abrupt* sags. Then, it leads to a less

severe peak values in the injected *abc* currents from the inverter. Indeed, the current peak value is 1.36 pu for *abrupt* unsymmetrical sag type F_1, while for *discrete* sag type F_1, the current peak value is 1.22 pu.

Finally, it should be noted that the aim of the paper is not to explain or to improve the control of a three-phase grid-connected inverter under voltage sags (as there is a lot of literature to this respect), but to show how the voltage recovery process have a strong influence on the injected currents by the inverter. Indeed, note from the results shown in Fig. 3 that if voltage sag is modelled abrupt, then the peak values of the injected currents after the voltage recovery are higher in the abrupt sag than in the discrete sag. It should also be noted that the filter's inductor tries to sooth the voltage sag effects. If this inductor where not placed in the filter, the time index of the current expression, i.e., L/R in the exponential term in (11) will be zero, which implies that the injected current will never reach its steady state value during the sag.

6. Sag parameters influence

The maximum (or peak) value of the injected current from the inverter to the grid is chosen as the variable to analyze the sag parameters influence. This variable (in pu) is obtained as:

$$i_{\text{max pu}} = \max\left\{|i_a(t)|, |i_b(t)|, |i_c(t)|\right\}\Big/\left(\sqrt{2}I_b\right) \qquad (18)$$

where I_b is the current base value ($I_b = I_N$, see Appendix I)

6

Table 2 Most unfavorable sag durations ($n = 0, 1, 2\ldots$)

| Symmetrical voltage sags			
A$_1$ (*abrupt*)	A$_1$ (*discrete*)	A$_4$ (*abrupt*)	A$_4$ (*discrete*)
$\Delta t = nT + 0.55T$	$\Delta t = nT + 0.55T$	$\Delta t = nT + 0.55T$	$\Delta t = nT + 0.64T$
Unsymmetrical voltage sags			
C	F$_1$ (*abrupt*)	F$_1$ (*discrete*)	F$_2$ (*abrupt*)	F$_2$ (*discrete*)
$\Delta t =$ $(n/2)\mathrm{T} + 0.72T$	$\Delta t =$ $n\mathrm{T} + 0.30T$	$\Delta t =$ $(n/2)\mathrm{T} + 0.30T$	$\Delta t =$ $n\mathrm{T} + 0.63T$	$\Delta t =$ $(n/2)\mathrm{T} + 0.63T$

and $i_a(t)$, $i_b(t)$ and $i_c(t)$ are the *abc* (or real) components of the currents injected from the inverter to the grid.

Fig. 4 shows the sag depth influence. All the simulated sags have a duration $\Delta t = 5.5$ cycles (i.e., 110 ms with $f = 50$ Hz) and the sag depth is varied from $0 \leq h \leq 1$, i.e., from the completely loss of voltage to the steady-state pre-fault voltage. Note that for both symmetrical sags (type A$_1$ and A$_4$) and unsymmetrical sags (type F$_1$ and F$_2$) the effects are less severe if the *discrete* voltage recovery process is considered. Certainly, the obtained curves for *abrupt* sags are always in a higher position than in the case of *discrete* sags, which means that the peak values of the injected currents will always be higher in the former than in the latter. Take the example of the sag depth $h = 0$: for symmetrical sag types A$_1$ and A$_5$ the peak current is around 5 pu if sag is modelled *abrupt*, while it is around 4 pu if sag is modelled *discrete*; for unsymmetrical sag types F$_1$ and F$_2$ the peak current is around 4 pu for *abrupt* sags, while for *discrete* sags this value is around 3 pu. Note also that for unsymmetrical sag type C there is no *discrete* recovery process, as Table 1 shows that the fault-clearing for this sag type is done in just one step (instantaneously).

Fig. 5 shows the sag duration influence. All the simulated sags have a depth $h = 0.8$ and the duration is varied from $5T \leq \Delta t \leq 7T$, i.e., from 5 to 7 cycles, which corresponds from 100 ms to 140 ms, with $f = 50$ Hz ($T = 20$ ms). From this figure, two conclusions can be drawn. On the one hand, *discrete* voltage sags originate less severe current peaks, as happened when studying the sag depth influence (Fig. 4). On the other hand, the sag duration influence is periodical, i.e., the current peaks for the most unfavourable sag durations are repeated either every cycle or half cycle. Table 2 shows the most unfavourable sag durations for each sag type, i.e., the durations that cause the highest current peaks in the inverter.

It should also be noted from the results shown in Sections V and VI that symmetrical sags cause the most severe effects on the inverter, as the injected currents have their highest peak values. Among unsymmetrical sags, it is observed that sag type F$_2$ causes the most severe effects and sag type C causes the less severe effects on the three-phase inverter.

Finally, it should be noted that this work has shown that when a voltage sag is produced in a power system, the way in which the voltage recovers has a strong influence on grid-connected inverters. The usual approach in the literature is to consider that the fault is cleared abruptly in all the affected phases. However, what it happens in real applications is that protections (e.g. circuit breakers) clear the fault in the natural zero-cross instants of the fault current, thus giving rise to a discrete fault-clearing process.
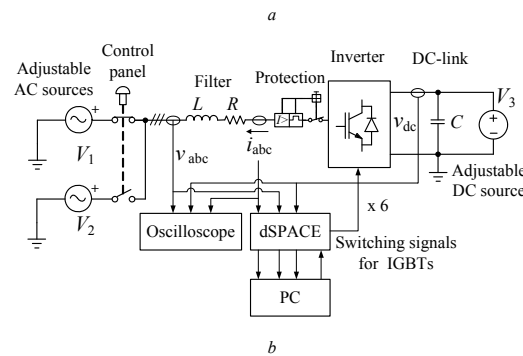

a

b
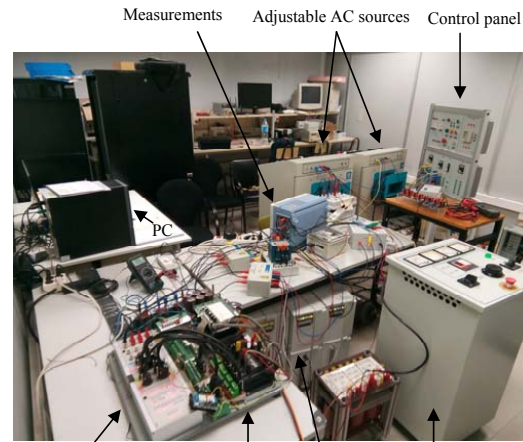
Fig. 6 *Experimental setup used to validate the analytical model and the simulation results of the three-phase inverter with RL filter under voltage sags*
a Real setup
b Electrical scheme

This paper has proposed a mathematical model for the three-phase grid-connected inverters under voltage sags, which describes their behaviour when either abrupt or discrete fault-clearing process take place. The simulations results have shown that a voltage sag modelled with an abrupt voltage recovery process overestimates the sag's severity, as the peak value of the injected currents is higher than in the real case (i.e. discrete voltage recovery process). So, the authors propose the use of discrete voltage sags when studying the behaviour of three-phase grid-connected inverters under voltage sags. In the following section, the analytical model and simulation results are validated by means of experimental tests.

7. Experimental results

The analytical model and the simulations results have been validated by means of the experimental setup shown in Fig. 6a. It consists of the following parts: two 6.4 kVA three-phase AC voltage sources and a control panel (with contactors and protections) to generate the voltage sag (emulating the grid); a 10 kVA three-phase inverter of
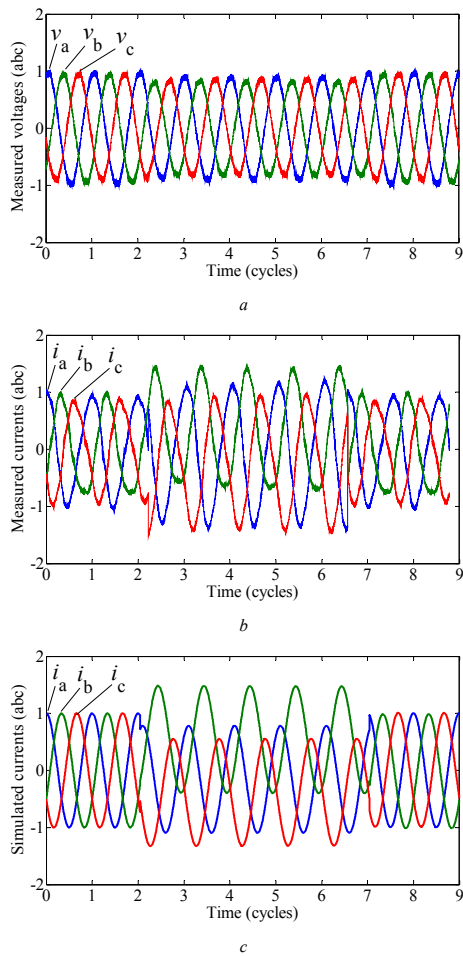
7

Fig. 7 *Three phase voltage sag effects on the injected current by the inverter.*
Sags characteristics: Δt = 5cycles, h = 0.9 and ψ = 86°

a Measured abc voltages (in pu)

b Measured abc currents (in pu)

c Simulated abc currents (in pu)

CINERGIA with a switching frequency of 20 kHz and DC link of 800 V with a capacitor of 1 mF; a three-phase *RL* filter with values 0.2 Ω and 10 mH; a 6.4 kVA voltage source that rectifies AC into DC voltage to generate the required voltage for the inverter's DC bus; voltmeters and ammeters connected to an oscilloscope, which registers the time evolution of the measured variables; and a dSPACE DS1104 of Texas Instruments for the double aim to send the measured voltages and currents to a PC (with the software MATLAB™) and to send the switching times for the three-phase inverter according to the desired control law.

The behaviour of the experimental setup can be explained by means of the electrical scheme depicted in Fig. 6b. The procedure to follow is explained below:

1) An adjustable three-phase AC source (V_1) is regulated to deliver 50 V (phase-to-phase voltage). This source emulates the grid.

2) An adjustable DC source (V_3) is regulated to deliver 180 V to the inverter's DC-link.

3) The inverter with RL filter is connected to the grid. Note that this inverter is safeguarded by means of an overcurrent protection.

4) The measuring devices read the values of the grid voltages (v_{abc}), the line currents (i_{abc}) and the DC-link voltage (v_{dc}), which are sent to an oscilloscope and to the dSPACE DS1104.

5) The dSPACE sends the measured real-time values to a PC with the MATLAB™ software, by means of which a PLL obtains the voltage angle in order to synchronize the inverter with the grid. The inverter is controlled to deliver 95 V (phase-to-phase voltage). Note that this voltage is higher than the grid voltage, so the current flows from the inverter to the grid.

6) Once the whole system is operating in steady-state conditions, a three-phase voltage sag with depth $h = 0.9$ is applied by pressing a button (from the control panel), which acts on two contactors. The first contactor is now open, so the V_1 source is disconnected from the system, while the second contactor is now closed, so the V_2 source is connected to the system. This source has been previously regulated to create the voltage sag with depth $h = 0.9$ from 50 V.

Fig. 7 shows the measured voltage and currents when applying a three-phase voltage sag (i.e. type A sag) with depth $h = 0.9$ and duration $Δt = 5$ cycles. The measured abc components of the grid voltages are depicted in Fig. 7a. It should be noted that the grid is not perfectly balanced, so that the measured abc components of the current, which are depicted in Fig. 7b, are not perfectly balanced in steady state conditions. Finally, Fig. 7c shows the abc components of the currents in the simulated case. It is observed that when the voltage sag originates, the injected current increases in order to keep constant the active power. This current increase is not critical, as the protection system did not act in the experimental test. If we compare the results shown in Fig. 7b and in Fig. 7c we can conclude that they are very similar: there is one phase (c phase) that has the highest peak values (because at the time instant when the sag starts, it corresponds to the c phase of the voltage, as shown in Fig. 7a). Finally, when the sag finishes, the system goes back to the steady-state regime. So, it can be concluded that the experimental results and the simulated ones correspond each other.

8. Conclusion

The present paper has developed an analytical model to study the behaviour of three-phase grid-connected inverters with *RL* filter under symmetrical and unsymmetrical voltage sags. The analytical results have been validated by simulations in MATLAB™ and by experimental results.

Voltage sags are usually modelled in the literature with *abrupt* (or instantaneous) voltage recovery, while in practice the voltage recovery process takes part in different steps (according to the natural zero crossing of the fault current), giving rise to *discrete* voltage sags. This work has shown that *abrupt* sags cause the most severe effects on three-phase

8

Table 3 Parameters of the studied system

DC-side		AC-side	
Renew. source	DC-link	Filter	Grid
$P = 50$ kW	$C = 18$ mF	$R = 1$ mΩ	$V_g = 400$ V (line)
$\cos \varphi = 1$	$V_{dc} = 1000$ V	$L = 4.9$ mH	$f = 50$ Hz

inverters, as they provoke the largest current peaks. In other words, *abrupt* sags overestimate the sag severity. Therefore, this paper proposes the use of *discrete* sags, because apart from being the real case, they are less severe than *abrupt* sags.

This paper has also shown that symmetrical sags are more severe than unsymmetrical sags, as they lead to the largest current peaks. Among unsymmetrical sags, the most severe is *abrupt* sag type F_2 and the least severe is type C.

An in-depth analysis considering all sag depths and durations has been carried out, showing two effects. On the one hand, *discrete* sags are less severe than *abrupt* sags, as they cause the largest current peaks injected from the inverter. On the other hand, the sag duration effects are periodical, i.e., the largest current peaks are obtained periodically. Moreover, it has also been observed that the largest peak currents are obtained not during sag but after voltage recovery, as depending on sag duration the value of the current could be closer or further from its pre-fault steady-state value. So, each sag type has its most unfavourable sag durations, which should be taken into account when proposing a suitable control algorithm to tackle the problem.

Finally, this preliminary study could be used to propose more robust control algorithms, which would let three-phase inverters with *RL* filter meet fault ride-through requirements.

9. References

[1] National Renewable Energy Laboratory (NREL): 'Renewable energy futures study. Vol. 1: Exploration of High-Penetration Renewable Electricity Futures', Tech. Report, 2012. Available: https://www.nrel.gov/

[2] Bollen, M.H.J.: 'Understanding power quality problems: voltage sags and interruptions' (IEEE Press, New York, 2000)

[3] Pedra, J., Sáinz, L., Córcoles, F., Guasch, L.: 'Symmetrical and unsymmetrical voltage sag effects on three-phase transformers'*, IEEE Trans. Power Deliv.*, 2005, 20, (2), pp. 1683-1691

[4] Pedra, J., Sáinz, L., Córcoles, F.: 'Effects of symmetrical voltage sags on squirrel-cage induction motors', *Elec. Power Syst. Res.*, 2007, 77, (12), pp. 1672-1680, Oct. 2007

[5] Pedra, J., Córcoles, F., Sáinz, L.: 'Effects of unsymmetrical voltage sags on squirrel-cage induction motors', *IET Gener. Transm. Distrib.*, 2007, 1, (5), pp. 769-775

[6] Bogarra, S., Rubión, X., Rolán, A., Córcoles, F., Pedra, J., Iglesias, J.: 'Small synchronous machine protection during voltage sags caused by MV grid faults', *Elec. Power Syst. Res.,* 2018, 156, (1), pp. 1-11

[7] Teodorescu, R., Liserre, M., Rodríguez, P.: 'Grid converters for photovoltaic and wind power systems' (John Willey & Sons, Chichester, 2011)

[8] IEEE Std. 1159-2009: 'IEEE Recommended Practice for Monitoring Electric Power Quality', IEEE, 2009

[9] Bollen, M.H.J.: 'Voltage recovery after unbalanced and balanced voltage dips in three-phase systems', *IEEE Trans. Power Deliv.*, 2003, 18, (4), pp. 1376-1381

[10] Rolán, A., Córcoles, F., Pedra, J., Monjo, Ll., Bogarra, S.: 'Testing of three-phase equipment under voltage sags', *IET Elec. Power App.*, 2015, 9, (4), pp. 287-296

[11] Reznik, A., Simöes, M.G., Al-Durra, A., Muyeen, S.M.: 'LCL filter design and performance analysis for grid-interconnected systems', *IEEE Trans. Ind. App.*, 2014, 50, (2), pp. 1225-1232

[12] Park, R.H.: 'Two-reaction theory of synchronous machines - Generalized method of analysis, Part I', *AIEE Transactions*, 1929, 48, pp. 716-727

[13] Chung, S.: 'A phase tracking system for three phase utility interface inverters', *IEEE Trans. Power Elec.*, 2000, 15, (3), pp. 431-438

[14] Bose, B.K.: 'Modern power electronics and ac drives' (Prentice Hall, New Jersey, 2002)

[15] Junyent-Ferré, A., Gomis-Bellmunt, O., Green, T.C., Soto-Sánchez, D.E.: 'Current control reference calculation issues for the operation of renewable source grid interface VSCs under unbalanced voltage sags', *IEEE Trans. Power Elec.*, 2011, 26, (12), pp. 3744-3753

[16] Akagi, H., Watanabe, E-H., Aredes, M.: 'Instantaneous power theory and applications to power conditioning' (2nd ed., IEEE Press, Hoboken, 2017)

[17] Ku, Y.H.: 'Transient analysis of AC machinery', *AIEE Transactions*, 1929, 48, pp. 707-714

[18] Fortescue, C.L.: 'Method of symmetrical co-ordinates applied to the solution of polyphase networks'. 34th Annual Convention of the AIEE, Atlantic City, New Jersey, USA; June 1918, pp. 1027-1140

10. Appendix 1: parameters of the studied system

Table 3 shows the parameters of the studied system, which consists of an AC-side (*RL* filter plus AC grid), and a DC-side (renewable energy source and DC-link).

11. Appendix 2: *Ku* transformation

The *Ku* transformation is used to obtain the transformed components of a given variable *x* from the *abc* components of this variable. Its power-invariant (or normalized) form is [17]:

$$\left[\mathbf{K}(\Psi) \right] = \frac{1}{\sqrt{3}} \begin{bmatrix} 1 & e^{j\Psi} & e^{-j\Psi} \\ 1 & a^2 e^{j\Psi} & a e^{-j\Psi} \\ 1 & a e^{j\Psi} & a^2 e^{-j\Psi} \end{bmatrix} \quad ; \quad a = e^{j2\pi/3} \tag{19}$$

$$\left[x_{abc} \right] = \left[\mathbf{K}(\Psi) \right] \left[x_{0fb} \right] \quad ; \quad \left[x_{0fb} \right] = \left[\mathbf{K}(\Psi) \right]^{-1} \left[x_{abc} \right]$$

where *x* is the studied variable (voltage, current or flux), the subscripts a, b and c stand for the *abc* components of the variable *x*, the subscripts 0, f and b stand for the *zero*, *forward* and *backward* components of the transformed variable *x*, and Ψ is the transformation angle. If the synchronous reference frame is used, then $\Psi = \omega t$, where $\omega = 2\pi f$ is the pulsation of the grid voltages (*f* is the grid frequency). Note that the *backward* (b) component is the complex conjugate of the *forward* (f) component, so only the latter is considered.

Let's assume an unbalanced system of three-phase voltages:

9

$$\underline{V}_a = V_a e^{j\varphi_{V_a}} \quad \rightarrow \quad v_a = \sqrt{2}V_a \cos\left(\omega t + \varphi_{V_a}\right)$$

$$\underline{V}_b = V_b e^{j\varphi_{V_b}} \quad \rightarrow \quad v_b = \sqrt{2}V_b \cos\left(\omega t + \varphi_{V_b}\right) \qquad (20)$$

$$\underline{V}_c = V_c e^{j\varphi_{V_c}} \quad \rightarrow \quad v_c = \sqrt{2}V_c \cos\left(\omega t + \varphi_{V_c}\right)$$

where $\underline{V}_a$, $\underline{V}_b$ and $\underline{V}_c$ are the phasors of the *abc* voltages, V_a, V_b and V_c are the modulus (rms values) of this phasors, φ_{Va}, φ_{Vb} and φ_{Vc} are the phase angles of the *abc* voltages and ω is the pulsation of the voltages. If the *Ku* transformation (19) is applied to (20), the transformed *forward* component results in:

$$v_f = \frac{e^{-j\omega t}}{\sqrt{3}}\left(v_a + av_b + a^2 v_c\right). \qquad (21)$$

Substituting (20) in (21) and taking into account the trigonometric relation $\cos(\alpha) = \left(e^{j\alpha} + e^{-j\alpha}\right)\big/2$ we have:

$$v_f = v_f^+ + v_f^- e^{-j2\omega t} \qquad (22)$$

where v_f^+ and v_f^- are given by:

$$v_f^+ = \frac{1}{\sqrt{6}}\left(V_a e^{j\varphi_{V_a}} + aV_b e^{j\varphi_{V_b}} + a^2 V_{sc} e^{j\varphi_{V_c}}\right)$$

$$v_f^- = \frac{1}{\sqrt{6}}\left(V_a e^{-j\varphi_{V_a}} + aV_b e^{-j\varphi_{V_b}} + a^2 V_c e^{-j\varphi_{V_c}}\right) \qquad (23)$$

Now, if we apply the *Fortescue* transformation [18] to the phasors in (20) we obtain their zero-, positive- and negative-sequence components (the zero component is neglected):

$$\underline{V}^+ = \frac{1}{3}\left(V_a e^{j\varphi_{V_a}} + aV_b e^{j\varphi_{V_b}} + a^2 V_c e^{j\varphi_{V_c}}\right)$$

$$\underline{V}^- = \frac{1}{3}\left(V_a e^{j\varphi_{V_a}} + a^2 V_b e^{j\varphi_{V_b}} + aV_c e^{j\varphi_{V_c}}\right). \qquad (24)$$

If we compare (24) with (23), it results in:

$$v_f^+ = \sqrt{3/2}\,\underline{V}^+ \qquad ; \qquad v_f^- = \sqrt{3/2}\left(\underline{V}^-\right)^* . \qquad (25)$$

Note that if (20) were a set of sinusoidal balanced voltages (steady-state conditions), then there will be no *negative*-sequence voltage, i.e., $v_f^- = 0$, and $\underline{V}^+$ would correspond to the steady-state phasor:

$$v_{f\,\text{steady state}} = \sqrt{3/2}\,\underline{V} = \sqrt{3/2}V e^{j\varphi_V} . \qquad (26)$$

Finally, the *Ku forward* component is related to the *Park dq* components as follows:

$$x_f = \frac{1}{\sqrt{2}}\left(x_d + jx_q\right) \rightarrow x_d = \sqrt{2}\,\mathrm{Re}\left(x_f\right); x_q = \sqrt{2}\,\mathrm{Im}\left(x_f\right). \quad (27)$$

10